nature neuroscience

Approach sensitivity in the retina processed by a multifunctional neural circuit

Thomas A Münch[1,3,4], Rava Azeredo da Silveira[2,4], Sandra Siegert[1], Tim James Viney[1], Gautam B Awatramani[1,3] & Botond Roska[1]

The detection of approaching objects, such as looming predators, is necessary for survival. Which neurons and circuits mediate this function? We combined genetic labeling of cell types, two-photon microscopy, electrophysiology and theoretical modeling to address this question. We identify an approach-sensitive ganglion cell type in the mouse retina, resolve elements of its afferent neural circuit, and describe how these confer approach sensitivity on the ganglion cell. The circuit's essential building block is a rapid inhibitory pathway: it selectively suppresses responses to non-approaching objects. This rapid inhibitory pathway, which includes AII amacrine cells connected to bipolar cells through electrical synapses, was previously described in the context of night-time vision. In the daytime conditions of our experiments, the same pathway conveys signals in the reverse direction. The dual use of a neural pathway in different physiological conditions illustrates the efficiency with which several functions can be accommodated in a single circuit.

In animals[1–5] and humans[6,7], approaching motion, such as that of looming objects, elicits well-documented behaviors, such as startle and protective motor responses. The relevance of approaching motion to survival, the requirement for rapid action upon the detection of an approach event and the stereotypical nature of motor responses all suggest the existence of dedicated neural hardware for the detection of approaching motion. Neurons have indeed been identified in locust[8–10] and in pigeon[11] that respond selectively to approaching motion stimuli. These are found in higher visual areas and seem to achieve a sophisticated whole-field computation that predicts the collision time of the looming object.

Here we describe an approach-sensitive neuron in the mammalian retina, namely a mouse ganglion cell type. We elucidate elements of its afferent circuit and show how these allow the approach-sensitive behavior of the ganglion cell. An important component of the circuit is a rapid inhibitory pathway that relies upon an electrical synapse. Finally, we summarize the mechanism of approach sensitivity in a computational model of a 'composite receptive field'. Experiments in frog[4,5] have suggested that approach detection may occur in the retina, but the mechanism there[4,5] seems to be different from the one we discuss here.

RESULTS

A ganglion cell type is sensitive to approaching motion

We recorded from ganglion cells, the output neurons of the retina, in transgenic mice ($Pvalb^{Cre} \times Thy1^{Stp\text{-}EYFP}$) in which a few ganglion cell types, and no other cell classes, were brightly labeled with enhanced yellow fluorescent protein (EYFP)[12,13] (**Fig. 1a**). We identified seven labeled ganglion cell types and denoted them PV-1 to PV-7 in order by depth of their dendritic arborizations within the inner plexiform layer (IPL). With a two-photon microscope, we distinguished these genetically labeled ganglion cells on the basis of their morphology and targeted them for recording. Here we discuss one OFF ganglion cell type, which we refer to as the PV-5 cell. The dendrites of this neuron arborized in the IPL at 80.6 ± 0.8% (n = 44; **Fig. 1b** top panel and **Supplementary Fig. 1**) relative to two strata marked by an antibody to choline acetyltransferase (ChAT)[14,15]. The dendritic tree of each PV-5 cell extended over a large area (diameter 350 ± 30 µm, n = 20; **Fig. 1b**, bottom panel), covering ~10° of the visual field. Unless otherwise noted, experiments were performed with PV-5 cells in isolated and light-adapted wholemount retinas.

We presented PV-5 cells with a set of stimuli that mimicked approaching motion (an expanding bar), lateral motion (a drifting bar) and receding motion (a shrinking bar) of a dark object within the dendritic field (**Fig. 1c**). All stimuli began with the presentation of a black bar at the center of the dendritic field. After a 2-s pause during which the image was held fixed, the two edges of the bar moved at different velocities to the left or to the right, drawn randomly from a set of velocities (**Fig. 1c**). Spiking responses were evoked preferentially by expanding bars compared to either drifting or shrinking bars (n = 7), at all velocities of the bar edges tested (**Fig. 1c**,**d**). The absent (or greatly reduced) response to non-approaching motion was not due to an overall change in the responsiveness of the cell during the course of the experiment, as the response to the onset of the black bar was similar for all stimuli (**Fig. 1c**). The peak spiking rate increased monotonically with edge velocity, while the spike count

[1]Neural Circuit Laboratories, Friedrich Miescher Institute for Biomedical Research, Basel, Switzerland. [2]Department of Physics and Department of Cognitive Studies, École Normale Supérieure, Paris, France. [3]Present addresses: Laboratory for Retinal Circuits and Optogenetics, Centre for Integrative Neuroscience, Eberhard-Karls University Tübingen, Tübingen, Germany (T.A.M.); Department of Anatomy and Neurobiology, Dalhousie University, Halifax, Nova Scotia, Canada (G.B.A.). [4]These authors contributed equally to this work. Correspondence should be addressed to B.R. (botond.roska@fmi.ch).

Received 24 November 2008; accepted 28 July 2009; published online 6 September 2009; doi:10.1038/nn.2389

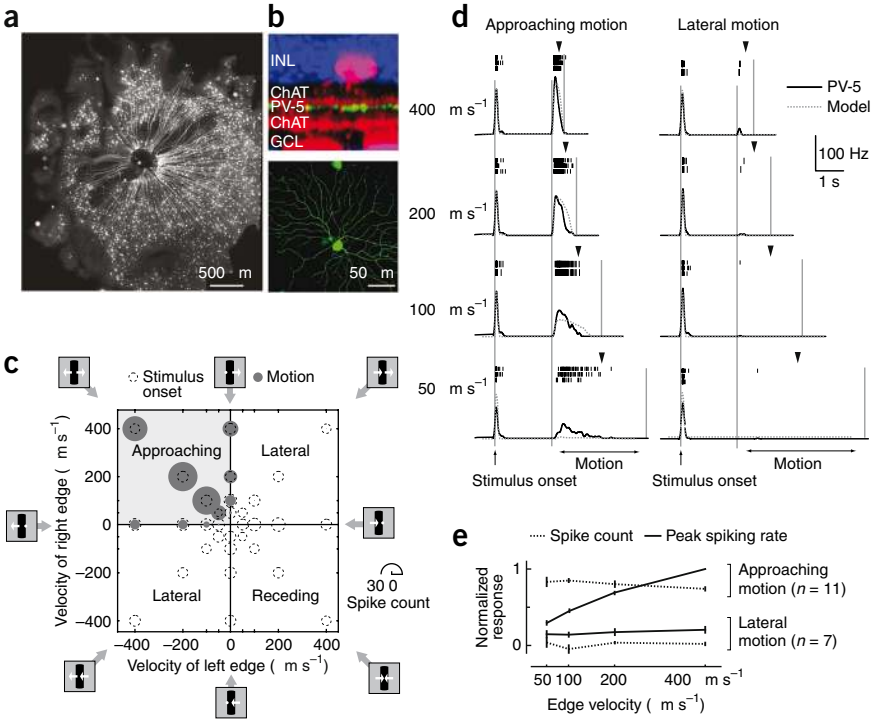

Figure 1 PV-5 ganglion cells are sensitive to approaching motion. (**a**) Wholemount retina from a *Pvalb*^{Cre} × *Thy1*$^{Stp\text{-}EYFP}$ mouse. Bright spots, ganglion cell somas; bright radial lines, axons extending toward the optic disc (central dark spot). (**b**) Side (top panel) and top (bottom panel) projections of a confocal image stack of a PV-5 cell, acquired after fixation. Green, neurobiotin-filled cell; red, ChAT; blue, DAPI; INL, inner nuclear layer; GCL, ganglion cell layer. (**c**,**d**) Spiking responses of a PV-5 cell to different motion stimuli. A 60-µm black bar was turned on within a 400-µm-diameter mask in the center of the dendritic field ("Stimulus onset"). After a 2-s pause, the left and the right edges of the bar began to move at velocities drawn at random from a number of values ("Motion"). (**c**) Overview of the responses over the parameter space. Radii of dotted circles and gray disks are proportional to the average spike count after the onset and during the motion of the bar, respectively. Scale radius is shown at lower right. The quadrant that corresponds to approaching motion is shaded in light gray. (**d**) Responses to expanding ("Approaching motion") and drifting ("Lateral motion") bars for different edge velocities. Ticks, individual spikes; black traces, average spiking rates; dotted gray traces, model outputs (**Supplementary Fig. 5**). Black arrowheads, times at which the moving edges exit the dendritic field of the cell. (**e**) Spike count and peak spiking rate during motion as a function of edge velocity, for expanding ("Approaching motion") and drifting ("Lateral motion") bars. Error bars, s.e.m.

during motion was roughly invariant (**Fig. 1e**). In summary, within the array of stimuli we used, PV-5 cells favored approaching motion over lateral and shrinking motion.

An approaching dark object results in a retinal image with both overall dimming and moving contrast edges. To dissect responses of PV-5 cells to these two components, we designed stimuli that distinguished overall dimming from the motion of contrast edges. First, we presented PV-5 cells with spatially uniform dimming stimuli with light levels matched to those of the approaching motion stimuli. As expected from an OFF cell, these purely dimming stimuli elicited significant responses in PV-5 cells (data not shown; $n = 4$). Next, we presented PV-5 cells with stimuli in which a bar expanded concomitantly with an overall brightening that maintained the total light intensity constant (**Fig. 2a**). Notably, PV-5 cells also responded significantly to this stimulus (**Fig. 2b**, $n = 6$). In summary, PV-5 cells responded not only to dimming, but also to the rapid expansion of a negative-contrast boundary within their dendritic field, even if it occurred in the absence of any dimming (**Fig. 2**).

Approach sensitivity relies upon a composite receptive field

We hypothesized that inhibitory activity was responsible for suppressing the response of PV-5 cells to non-approaching motion. To test this hypothesis, we recorded excitatory and inhibitory inputs during stimulation with different spatiotemporal patterns. When stimulated for 2 s with a dark spot (400-µm diameter, $n = 30$) against a gray background, PV-5 cells responded with a burst of spikes at the onset of this OFF (dimming) stimulus (**Fig. 3a**, top trace). Excitatory synaptic currents ('excitation'; see Online Methods), which follow glutamatergic inputs from bipolar cells[16–18], were also activated only at the onset of the stimulus (**Fig. 3a**, bottom trace; $n = 38$). By contrast, inhibitory synaptic currents ('inhibition'; see Online Methods), which follow inputs from amacrine cells[16–18], were evoked at the offset of the stimulus, when the dark spot was removed: effectively an ON (brightening) stimulus (**Fig. 3a**, middle trace; $n = 38$). Hence, PV-5 cells were excited at light decrements and inhibited at light increments. In the case of this simple stimulus, excitation and inhibition did not interact because they occurred at different times.

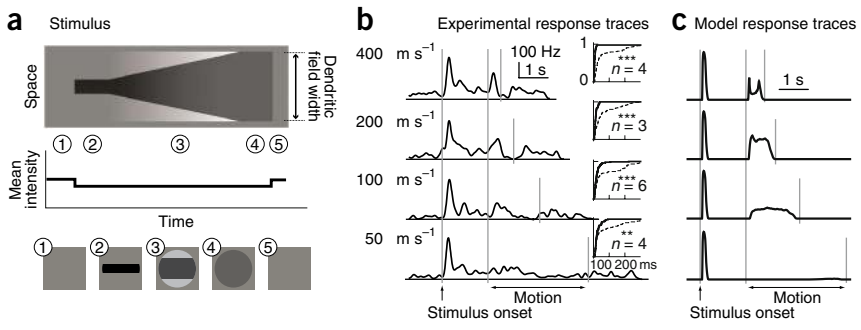

Figure 2 PV-5 ganglion cells respond to approaching motion even in the absence of dimming. (**a**) Illustration of the constant-luminance stimulus, which consisted of an expanding dark bar together with progressive overall brightening that maintained the overall light intensity constant. (**b**) PV-5 cell spiking rate in response to the stimulus illustrated in **a**. Insets, cumulative distributions of the interspike intervals during baseline activity (dashed lines) and during the first 500 ms of expansion (solid lines). $^{**}P < 0.01$, $^{***}P < 0.001$ (one-sided Kolmogorov-Smirnov test; *n*, number of stimulus repetitions). (**c**) Model output in response to the stimulus illustrated in **a**.

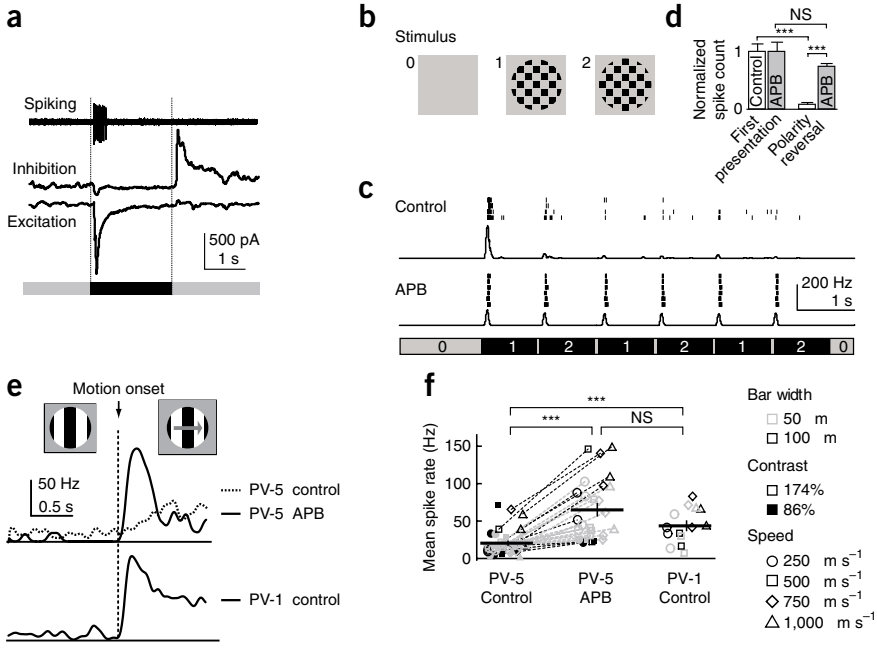

Figure 3 Response of PV-5 ganglion cells to lateral motion is suppressed by an ON inhibitory signal. (**a**) Spiking, excitation and inhibition responses of a PV-5 ganglion cell to a 400-μm-diameter black disk presented for 2 s (black bar at bottom). (**b**–**d**) Spiking responses to a polarity-reversing black-and-gray checkerboard (checker size, 50 μm). (**b**) Stimulus frames. (**c**) Top: responses in control conditions; bottom: responses under 80 μM APB. Ticks, individual spikes; black traces, average spiking rate; bottom row, stimulus frame sequence. (Thin gray lines between stimulus frames do not represent a stimulus; they are graphical separators only.) (**d**) Comparison of normalized spike count after the first presentation of the checkerboard and after polarity reversals, in control conditions and with APB. Error bars, s.e.m.; ***$P < 0.001$; NS, not significant (*t*-test). (**e**) Top: spiking rate responses of a PV-5 cell to the onset of lateral motion in control conditions and with APB (80 μM). Bottom: spiking rate response of a PV-1 cell to the onset of lateral motion under control conditions. (**f**) Mean spiking rate responses during the first 200 ms after onset of lateral motion, in PV-5 cells under control conditions and with APB (80 μM) and in PV-1 cells under control conditions. Dashed lines connect data points originating from the same cell stimulated with the same stimulus. Thick horizontal lines, mean responses of the cell populations. Thin vertical lines, s.e.m.; ***$P < 0.001$; NS, not significant (Mann-Whitney rank test).

The situation is different when OFF and ON stimuli appear simultaneously in different regions within the dendritic field. We presented PV-5 cells with a polarity-reversing checkerboard against a gray background (**Fig. 3b**). The initial presentation of the black checkerboard resulted in a net darkening, and consequently the ganglion cell fired a burst of spikes (**Fig. 3c**). At each reversal, half of the checkers became brighter and the other half became darker, such that there was no change in the mean light intensity across the

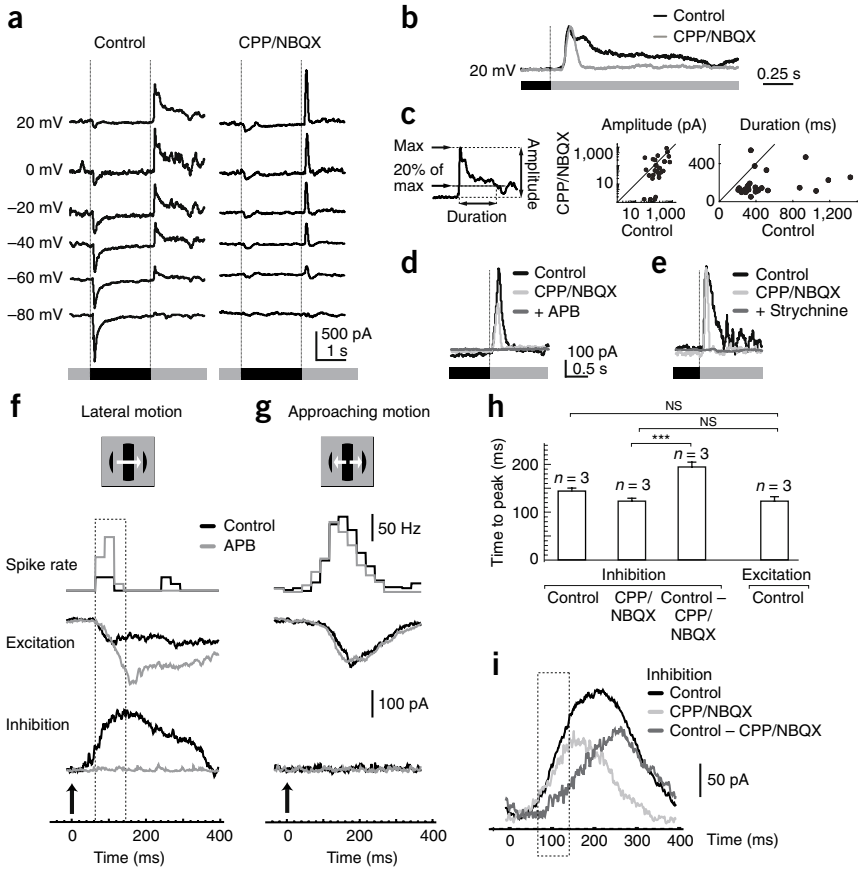

Figure 4 PV-5 ganglion cells receive a rapid inhibitory input required to suppress responses to lateral motion. (**a**) Synaptic currents at various holding potentials, in response to a 400-μm black disk presented for 2 s. Left, control; right, CPP/NBQX. (**b**) Inhibitory currents from **a** at a finer temporal resolution. Peak amplitudes are normalized. (**c**) Left, trace of inhibitory current, displayed to illustrate the definitions of 'amplitude' and 'duration'. Middle and right, amplitude and duration of the inhibitory currents in control conditions and with CPP/NBQX. (**d**,**e**) Effects of APB (**d**, 80 μM) and strychnine (**e**) on the rapid inhibitory current isolated by CPP/NBQX. (**f**,**g**) Responses to lateral (**f**) and to approaching (**g**) motion in control conditions and with APB (10 μM). The stimulus, presented within a 300-μm-diameter mask, was a black-and-gray grating (100-μm bar width) with edges moving at 500 μm s^{-1}. Dashed box in **f**, duration of the burst of spikes; arrows, motion onset. (**h**) Time to peak of the different components of the excitatory and inhibitory inputs in PV-5 cells presented with the same stimulus as in **f**. 'Time to peak' is the delay, counting from stimulus onset, before the response reaches 67% of its peak. 'Control – CPP/NBQX' is the CPP/NBQX-blocked component. Error bars, s.e.m.; ***$P < 0.001$; NS, $P \geq 0.05$. (**i**) Inhibitory input in response to the same stimulus as in **f**, showing the relative timing of the CPP/NBQX-resistant component (light gray) and the CPP/NBQX-blocked component (dark gray). Dashed box as in **f**.

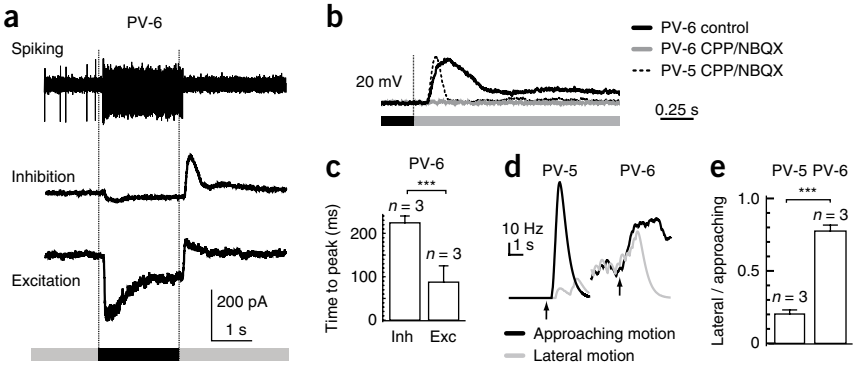

Figure 5 PV-6 OFF ganglion cells respond to lateral motion. (**a**) Spiking activity, as well as excitatory and inhibitory inputs, in a PV-6 ganglion cell, in response to a 400-µm-diameter black disk presented for 2 s. (**b**) Inhibitory currents in PV-6 cells, in control conditions and with CPP/NBQX. For comparison, the CPP/NBQX-resistant component of the inhibitory input to PV-5 cells is reproduced from **Figure 4b**. Peak amplitudes are normalized to emphasize the relative timing of the responses. (**c**–**e**) Responses to a black-and-gray grating (100-µm bar width), with edges moving at 500 µm s^{-1}, within a 300-µm-diameter mask. (**c**) Time to peak of excitatory and inhibitory currents in PV-6 cells during lateral motion. (**d**) Spiking rates in PV-5 and PV-6 cells, in response to lateral motion and to approaching motion. Arrows, motion onset. (**e**) Ratio of peak spiking rate responses to lateral motion and approaching motion, in PV-5 and in PV-6 cells. Error bars, s.e.m.; ***$P < 0.001$.

PV-5 cell dendritic field. These reversals elicited very little spiking in PV-5 cells under control conditions (**Fig. 3c**, top panel; **Fig. 3d**; $n = 5$). By contrast, when the ON pathway was blocked with 80 µM APB (L-(+)-2-amino-4-phosphonobutyric acid)[19], PV-5 cells responded at each polarity reversal (**Fig. 3c**, bottom panel; **Fig. 3d**). Hence, in control conditions ON inhibition suppressed the spiking response (see also **Supplementary Fig. 2**). ON inhibition influenced not only the spiking activity but also the magnitude of the excitatory input (**Supplementary Fig. 2b**, $n = 5$). Our interpretation of this finding is that ON inhibition acts both on PV-5 cells directly and on OFF bipolar cell terminals. These results suggest a composite receptive field, made up of many 'push-pull' (OFF excitation, ON inhibition) subunits[20,21] that can interact when their outputs are pooled by the ganglion cell.

The composite nature of the receptive field could explain the sensitivity of PV-5 cells to approaching stimuli. Approaching motion of a dark object would result in an OFF stimulus and, consequently, excitation without inhibition. By comparison, receding motion would result in an ON stimulus and, consequently, inhibition without excitation. Lateral motion of a dark object would result in a leading OFF stimulus and a trailing ON stimulus and, consequently, both excitation and inhibition, which interact because they occur concomitantly.

We used drifting gratings, displayed within a mask of 300-µm diameter, to investigate the putative inhibitory suppression of responses to lateral motion (**Fig. 3e**,**f**). When we blocked ON inhibition with APB, a vigorous spiking response appeared at the onset of motion that was not observed in control conditions (**Fig. 3e**, top panel, $n = 5$). This result indicates that ON inhibition serves to suppress responses of PV-5 cells to lateral motion. The suppression was robust: we observed it for a variety of spatial frequencies, grating contrasts and drifting velocities (**Fig. 3f**). It was instructive to compare the behavior of PV-5 cells to that of the similarly large (360 ± 70 µm, $n = 6$) and transient PV-1 cells. PV-1 cells stratified at −40 ± 4% (**Supplementary Fig. 1b**) and received fast ON excitation and slow ON inhibition (data not shown). Hence, their receptive field was not composed of push-pull subunits. PV-1 cells did respond to the onset of lateral motion (**Fig. 3e** bottom panel and **Fig. 3f**, $n = 3$). This comparison supports the claim that the presence of push-pull subunits in the composite receptive field of PV-5 cells is responsible for the suppression of responses to undesired stimuli.

Rapid inhibition is involved in approach sensitivity

A key aspect of the approach-sensitivity mechanism not discussed thus far pertains to dynamics: suppression of the response to non-approaching stimuli occurs only if ON inhibition acts sufficiently rapidly to cancel OFF excitation. We analyzed the temporal structure of synaptic inputs under the effect of blockers of ionotropic glutamate receptors (CPP/NBQX: 10 µM (±)-3-(2-Carboxypiperazin-4-yl) propyl-1-phosphonic acid, blocking NMDA receptors; plus 10 µM 6-nitro-2,3-dioxo-1,4-dihydrobenzo[f]quinoxaline-7-sulfonamide, blocking AMPA and kainate receptors). CPP/NBQX abolished the excitatory input (**Fig. 4a**; $n = 29$). However, a rapid inhibitory signal remained (**Fig. 4a–c**; $n = 24$ of 29 cells), with comparable amplitude to that recorded in the control experiment (**Fig. 4c**: 84% ± 47% of control; $n = 24$, $P = 0.38$, paired t-test). This CPP/NBQX-resistant, rapid inhibition was blocked by APB (10 µM, $n = 4$, or 80 µM, $n = 4$; **Fig. 4d**) and also by strychnine (10 µM, $n = 3$; **Fig. 4e**), a glycinergic receptor antagonist. Curare (50 µM, $n = 3$), a nicotinic acetylcholine receptor antagonist, and SR-95531 (5 µM; $n = 3$), a $GABA_A$ receptor antagonist, had no effect on the rapid inhibition (data not shown).

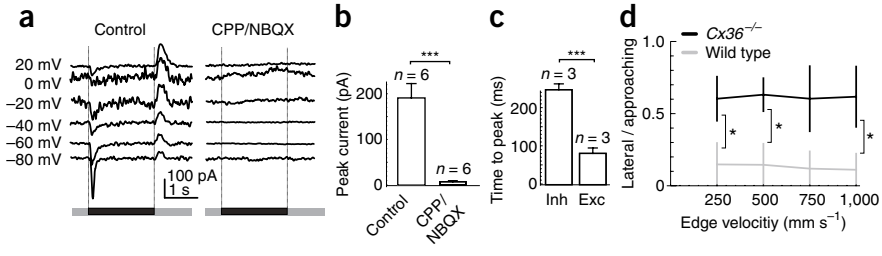

Figure 6 The rapid inhibitory pathway is mediated by an electrical synapse. Unless noted, all traces on this figure are from PV-5 cells in *Cx36*$^{-/-}$ background. (**a**) Synaptic currents at various holding potentials in response to a 400-µm black disk presented for 2 s in control conditions and with CPP/NBQX. (**b**) Effect of CPP/NBQX on the magnitude of the inhibition. (**c**) Time to peak of inhibitory (Inh) and excitatory (Exc) currents. Stimulus, presented within a 300-µm-diameter mask, was a black-and-gray grating (100-µm bar width), with edges moving at 500 µm s^{-1}. (**d**) Ratio of peak spiking rate responses to lateral motion and approaching motion, for different edge velocities, in *Cx36*$^{-/-}$ and wild-type mice. The P-value at 750 µm s^{-1} was 0.0502, only slightly above significance level 0.05. Error bars, s.e.m.; *$P < 0.05$, ***$P < 0.001$.

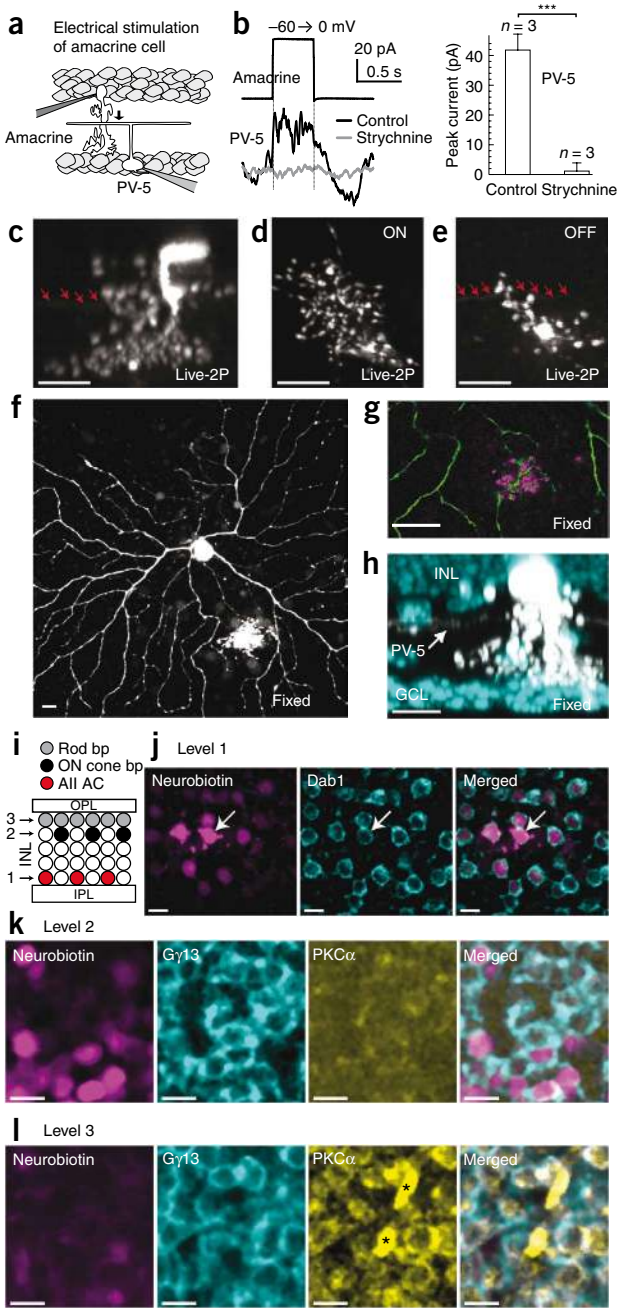

Figure 7 PV-5 cells receive an inhibitory input from AII amacrine cells. (**a**) Schematic of a double-patch experiment (side view). The experiment was performed on wholemount retina. (**b**) Left, inhibitory currents in a PV-5 cell (black, control; gray, strychnine) evoked by stimulating the double-patched amacrine cell. Right, peak inhibitory currents in PV-5 cells after amacrine cell stimulation. Error bars, s.e.m.; $***P < 0.001$. (**c**–**e**) Two-photon (2P) images of a presynaptic amacrine cell in a double patch. Red arrows, dendrite of the connected PV-5 cell. (Images overexposed to show dim signal are in **Supplementary Fig. 4**.) (**c**) Side projection. (**d**) Top projection of proximal IPL. (**e**) Top projection of distal IPL. (**f**) Maximum intensity projection of a confocal stack of a recorded amacrine–PV-5 cell pair. (**g**) Confocal section at higher magnification. Magenta, pixels with neurobiotin staining only; green, pixels with neurobiotin and EYFP staining. (**h**) Magnified side view from **f**. Cyan, DAPI. (**i**) Schematic representation of cell bodies in the inner nuclear layer (INL). Rod bp, rod bipolar cells; ON cone bp, ON cone bipolar cell; AII AC, AII amacrine cell. Levels refer to the depths of confocal sections marked in **j**–**l**. (**j**) A recorded and neurobiotin-filled (magenta) amacrine cell (level 1) in a double-patch experiment (arrow). Dab1 staining, cyan. (**k**) Neurobiotin-labeled cells (magenta), in level 2, are positive for Gγ13 (cyan) and negative for PKCα (yellow). (**l**) No neurobiotin-labeled cells (magenta) are present in level 3, where most cells are positive for Gγ13 (cyan) and PKCα (yellow). The secondary antibody to mouse also labels blood vessels (asterisks). Scale bars, 10 μm.

The pharmacological actions of all blockers used in our experiments were reversible (data not shown). These experiments suggest that a three-synapse pathway (**Supplementary Fig. 3a**) carries the rapid inhibitory component: cones to ON bipolar cells, ON bipolar cells to amacrine cells through a conduit unimpaired by CPP/NBQX and amacrine cells to PV-5 ganglion cells through glycine receptors. By contrast, the excitatory pathway seems to be conventional: cones to OFF bipolar cells, and OFF bipolar cells to the PV-5 cell through ionotropic glutamate receptors.

Inhibition must act rapidly enough to prevent spiking in PV-5 cells presented with lateral motion. We compared the timing of spiking responses, excitatory inputs, and inhibitory inputs of PV-5 cells stimulated with moving black-and-gray gratings (100-μm-wide bars at a speed of 500 μm s^{-1}), both in control conditions and when the ON pathway was blocked (**Fig. 4f**,**g**, 10 μM APB; $n = 3$). We found, first, that during lateral motion the excitatory and the inhibitory currents occurred with similar time courses in control conditions (**Fig. 4f**,**h**). Second, when inhibition was blocked with APB, a burst of spikes appeared at the onset of lateral motion. Notably, the timing of this burst of spikes was comparable to that of the rapid component of inhibition, which was blocked by APB (**Fig. 4f**). We also observed that the presence of APB enhanced the excitatory input (**Fig. 4f**), an effect already noted in the context of the checkerboard stimuli (**Supplementary Fig. 2b**). By contrast, during approaching motion, no inhibition was detected in control conditions and APB had no effect on the spiking and excitatory responses (**Fig. 4g**, 10 μM APB; $P = 0.65$ for spiking and $P = 0.7$ for excitation, t-test; $n = 3$). These results are consistent with the notion that rapid, ON-inhibitory signal blocks spiking at the onset of lateral motion.

PV-5 cells receive both CPP/NBQX-blocked and CPP/NBQX-resistant inhibitory inputs, but the CPP/NBQX-resistant component occurs over a significantly shorter time scale than the blocked component (**Fig. 4h**,**i**). Within the time window defined by the burst of spikes that follows the onset of lateral motion (recorded in the presence of APB), 80 ± 6% of the inhibitory signal ($n = 4$, quantified as the integral of the inhibitory current over time) was CPP/NBQX-resistant. This finding suggests that the CPP/NBQX-resistant inhibitory pathway dominates in the suppression of PV-5 cell responses to the onset of lateral motion.

The relevance of rapid inhibition to the PV-5 cell physiology was also apparent when we compared this cell to another EYFP-labeled OFF cell in the $Pvalb^{Cre} \times Thy1^{Stp\text{-}EYFP}$ mouse line, which we called the PV-6 cell. Similarly to the PV-5 cell, the PV-6 cell had a wide dendritic field (diameter 400 ± 40 μm, stratification at 125 ± 8%, $n = 6$) and received OFF excitation and ON inhibition (**Fig. 5a**, $n = 6$). However, the inhibitory input to PV-6 cells was slower than that observed for PV-5 cells, and it was entirely blocked by CPP/NBQX (**Fig. 5b**; $n = 3$). The PV-6 cell circuit was therefore devoid of a rapid inhibitory pathway. Excitation was faster than inhibition in PV-6 cells (**Fig. 5c**) and, unlike PV-5 cells, these cells responded to both approaching and lateral motion (**Fig. 5d**,**e**). The contrast between the physiology of PV-5 cells and PV-6 cells further supports the relevance of the CPP/NBQX-resistant inhibitory component in the mechanism of approach sensitivity.

In the rapid inhibitory pathway, the excitatory synapse between the ON cone bipolar cell and the amacrine cell is neither glutamatergic

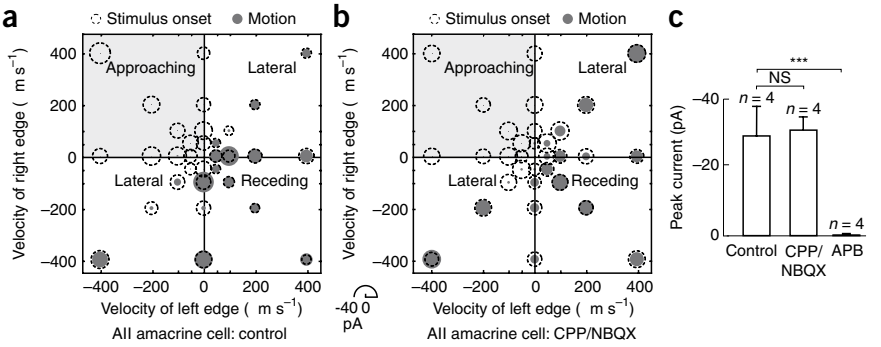

Figure 8 The functional properties of AII amacrine cells are consistent with the rapid inhibitory signal in PV-5 ganglion cells. (**a**,**b**) Motion-response map of an AII amacrine cell in control conditions (**a**) and with CPP/NBQX (**b**). Map is analogous to that in **Figure 1c**. The recorded cell was clamped to −60 mV. The radii of the disks are proportional to the peak magnitudes of inward currents evoked by stimulus motion. The radii of the dotted circles are proportional to the reduction of the excitatory currents after the initial presentations of the black bar. The quadrant that corresponds to approaching motion is shaded in light gray. (**c**) Average peak magnitudes of excitatory currents in AII amacrine cells, in the lateral and receding quadrants of the motion-response map, under different pharmacological conditions (CPP/NBQX and 10 μM APB). Error bars, s.e.m.; $***P < 0.001$; NS, $P \geq 0.05$.

nor cholinergic, but it may be electrical. Electrical synapses consist of connexin proteins, of which connexin36 (Cx36) is one of the most abundant in the mouse retina[22–24]. In mice lacking Cx36 ($Cx36^{-/-}$) CPP/NBQX blocked the excitatory and inhibitory inputs to PV-5 cells (**Fig. 6a**,**b**). Inhibition was slower than excitation (**Fig. 6c**), and the ability of the PV-5 cell to discriminate between approaching and lateral motion in the $Cx36^{-/-}$ background was inferior to that in wild type for three of four velocities tested (**Fig. 6d**, $n = 3$). These observations, together with the pharmacological observations described above, indicate that rapid inhibition transits between ON cone bipolar cells and amacrine cells through an electrical synapse (**Supplementary Fig. 3a**) that requires functional Cx36.

The approach-sensitive neural circuit is multifunctional

The circuit element responsible for the rapid inhibitory input to PV-5 cells—namely, an ON cone bipolar cell connected by a Cx36-containing electrical synapse to a glycinergic amacrine cell—is reminiscent of the rod pathway circuitry[22–25]. During scotopic (night-time) vision, the glycinergic AII amacrine cells[26], after activation by rod bipolar cells, transmit signals through Cx36-containing electrical synapses to ON cone bipolar cells[22–24,27]. An attractive hypothesis is that the rapid inhibitory pathway afferent to PV-5 cells makes use of the same electrical synapse as the one associated with the rod circuit, but with a reversed information flow[15,28–31] (**Supplementary Fig. 3b**). As a direct test of this hypothesis, we performed dual-patch recordings of amacrine cells and PV-5 ganglion cells in flatmount retinas (**Fig. 7a**). We targeted amacrine cells in the most proximal sublayer of the inner nuclear layer (INL), where we estimated that roughly one-third of the cells were AII amacrine cells. This estimation was based on antibody staining for Dab1, a selective AII amacrine cell marker[32]. We recorded from 16 amacrine–PV-5 cell pairs. In six pairs, depolarizing voltage steps applied to the amacrine cell elicited inhibitory currents in the PV-5 ganglion cell (**Fig. 7b**). The rapid component of these inhibitory currents survived the application of CPP/NBQX ($n = 3$), reflecting direct input from the stimulated cell (data not shown). Strychnine abolished the inhibitory currents in PV-5 cells that were otherwise elicited by amacrine cell stimulation in control conditions (**Fig. 7b**; $n = 3$). From this observation, we inferred that the inhibitory transmission used glycine receptors.

To determine the identity of the six amacrine cells that evoked inhibitory currents in PV-5 cells when they were electrically stimulated, we visualized the morphology of three of these cells under the two-photon microscope after the recordings (**Fig. 7c–e** and **Supplementary Fig. 4**), and all six cells by confocal fluorescence microscopy *post hoc* in fixed retinas (**Fig. 7f–h**). The narrow-field (cell lateral diameter 26 ± 2 μm; $n = 6$), vertically oriented morphology, with small boutons in the ON layer and larger lobules in the OFF layer, suggested that the recorded cells were AII amacrine cells (**Fig. 7c–h**). For verification, we double-stained three of the six amacrine cells with anti-Dab1 (**Figs. 7i**,**j**). In all three cases, the recorded cells were positive for Dab1. Moreover, tracer-coupled cells in the vicinity of the recorded amacrine cells, in the same nuclear layer, were also Dab1 positive. This result suggested coupling between neighboring AII amacrine cells (**Fig. 7j**). Tracer-coupled somas were also detected in more distal nuclear layers within the INL, and, therefore, we tested in the three other pair-recorded amacrine cells (that evoked inhibition in PV-5 cells) whether the distally coupled cells might be ON cone bipolar cells. ON cone bipolar cells can be identified through labeling with an antibody recognizing the marker Gγ13 (ref. 33) and can be differentiated from rod bipolar cells because they do not stain for the marker PKCα (ref. 34). In all three samples we examined, the tracer-coupled cells in the distal INL were Gγ13-positive and PKCα-negative (**Fig. 7k**,**l**). We therefore concluded that the cells in the distal INL tracer-coupled with AII amacrine cells were indeed ON cone bipolar cells.

We completed the analysis of the approach-sensitive circuit by measuring the response of AII amacrine cells presented with the same stimulus array used for probing PV-5 cells (**Fig. 1c**). AII amacrine cells were recorded under voltage clamp conditions (at −60 mV). After the recordings, AII amacrine cells were identified by their morphology using two-photon laser microscopy and staining with the Dab1 antibody (data not shown). As expected, light increments evoked excitatory currents in AII amacrine cells, but light decrement did not (traces not shown). The response map of AII amacrine cells ($n = 4$) in control conditions and under CPP/NBQX treatment showed a pattern complementary to the response map of PV-5 cells (**Fig. 8a**,**b**). Furthermore, during lateral motion and receding motion, CPP/NBQX blocked the slow component of the excitatory input but did not affect its rapid component (data not shown). APB, however, abolished the response of AII amacrine cells to both stimulus onset and lateral motion (**Fig. 8c**). These results indicate that AII amacrine cells provide the rapid component of the inhibition, as well as a portion, or possibly the entirety, of the slow inhibitory input to PV-5 cells.

Computational model of approach sensitivity

We incorporated the various elements of the proposed composite receptive field of the PV-5 cell into a computational model (**Supplementary Fig. 5**). The model PV-5 cell sums over a large region covered by many push-pull subunits (**Supplementary Figs. 5a**,**b**) that excite the PV-5 cell in response to local OFF inputs and inhibit it

in response to local ON inputs. The two processes—excitation and inhibition—occur with similar dynamics (**Supplementary Fig. 5c**). As a result, inhibition prevents responses to undesired stimuli (such as the laterally moving object in **Supplementary Fig. 5b**).

As a key element, signals from subunits are rectified before being summed by the PV-5 cell (**Supplementary Fig. 5c**). Because of this concave nonlinearity, strong local signals are favored over weak diffuse ones. Thus, the model PV-5 cell responds to the expanding edges of an approaching object even if the visual field undergoes slow brightening so as to prevent overall dimming (such as in **Fig. 2a**). The computational model reproduces the data (**Figs. 1d** and **2c**) and closely follows experimental traces for an array of input patterns and velocities.

DISCUSSION

Retinal analysis of motion

In the retina, visual information is broken up and transmitted in parallel channels to central brain regions by different types of ganglion cells. An appreciable fraction of retinal circuitry is devoted to the analysis of different categories of motion. In addition to the approach-sensitive ganglion cell type described here, eight types of direction-selective ganglion cells (four ON-OFF types[35], three ON types[35] and one OFF type[13]) report either the direction of lateral object motion or the direction of global image drift. Still other ganglion cell types respond to differential object motion relative to global background motion[36].

In all three cases of motion sensitivity—direction selectivity[13,35], differential-motion sensitivity[36] and approach sensitivity—the ganglion cells respond most vigorously to a so-called preferred stimulus, whereas their responses to so-called null stimuli are suppressed. The preferred stimuli are object motion in a given direction, differential object-background motion and approaching motion, respectively, whereas null stimuli are motion in the opposite direction, coherent object-background motion and receding or lateral motion, respectively. But ganglion cells are broadly tuned, and 'sensitivity' does *not* mean 'exclusivity': motion-sensitive cells do not respond to their preferred stimulus alone. For example, an OFF direction-selective, differential motion-sensitive, or approach-sensitive cell will respond vigorously to a dark flash, like any other OFF ganglion cell. The essence of motion sensitivity lies in the suppression of responses to null stimuli; that is, in what the motion-sensitive cell does not respond to.

The approaching motion of an object was mimicked in our experiments by an expanding bar projected onto a fixed retina. In natural situations, an expanding retinal image can result from either object motion or observer motion. The PV-5 cell may distinguish these two situations. When an observer moves toward a static scene, one expects the retinal image to comprise many concomitantly expanding dark and bright areas (along with lateral drift). According to our model, these lead to both excitation and inhibition, which cancel each other, and, hence, we expect a weak or negligible response. Thus, PV-5 cells may be more responsive to true object motion than to apparent motion in the visual field due to observer motion.

Scales and ambiguities in approach sensitivity

We have referred to the retinal PV-5 ganglion cell as an 'approach-sensitive' cell and thereby differentiated it from the 'looming-sensitive' cells observed in higher brain centers of locust[8] and pigeon[11]. Besides their location in the visual stream, approach- and looming-sensitive cells differ by the scales of their receptive fields and in the nature of the information they encode. They may also differ in the way in which they handle visual ambiguities.

PV-5 cells may fulfill an 'alert function'[37] by signaling approaching motion, such as that of a falcon aiming at a mouse, to higher brain centers. Looming-sensitive cells in locust brain have spatial and functional properties that are different from PV-5 cells. The receptive fields of looming-sensitive cells are larger than those of PV-5 cells[8–11]. Their response is also more sophisticated in that they can respond to object approach independent of the object contrast and in that they encode the time of collision (between the approaching object and the observer) in the temporal structure of the spiking rate. In PV-5 cells, we found a simple correlation between the velocity of an approaching object and the spiking rate (**Fig. 1e**). PV-5 cells may serve as elementary building blocks in motion-sensing streams: their outputs may be pooled by downstream detectors, such as looming-sensitive cells, that cover a wider field. Furthermore, by combining information from several approach-sensitive cells, higher-order cells may achieve more involved spatiotemporal computations.

One kind of putative spatiotemporal computation that would be useful relates to the resolution of visual ambiguities. Any procedure that aims at inferring a three-dimensional trajectory from its two-dimensional (retinal) projection faces ambiguity. In the case of PV-5 cells, approaching dark objects can be confused with receding bright objects (for example, a bright, narrowing gap between two large, approaching objects). Ambiguities may also arise when object motion occurs near the edge of a cell's receptive field—a special case of the well-known 'aperture problem'[38]. For example, a large object that enters the receptive field laterally may be confused with an approaching object. All these are fundamental ambiguities pertaining to the stimulus, which cannot be resolved by the PV-5 cell. Instances of the aperture problem may be solved by the use of a receptive field covering the entire visual scene. More often, the resolution of visual ambiguities necessitates the integration of information coming from several 'elementary' cells such as approach-sensitive ones. So, here again PV-5 cells come into the picture as candidate building blocks that can feed useful information to higher-order cells.

Implementation of approach sensitivity

The PV-5 cell receives excitatory and inhibitory inputs from small subunits, namely bipolar (excitatory) and bipolar–amacrine (inhibitory) circuits. The excitatory subunits are of the OFF type, and the inhibitory subunits are of the ON type. This push-pull[20,21] structure, taken together with the finding that excitatory and inhibitory subunit responses follow similar time courses, ensures that concomitant bright and dark inputs of comparable intensity 'cancel' each other and, hence, trigger no appreciable PV-5 cell response. This explains the insensitivity to lateral motion: trailing (ON) edges inhibit the excitatory effect of leading (OFF) edges.

As for the sensitivity to approaching motion, the key point is that the PV-5 cell receptive field is large and 'composite': it sums over many ON-OFF subunits, and this integration is nonlinear. The responses of individual subunits are thresholded by a concave nonlinearity, and the outcomes of this operation are then summed linearly into a global ganglion cell input. When the PV-5 cell is presented with an approaching dark object, the moving image on the retina is that of an expanding dark area. In a sense, there is no 'trailing' edge, but everywhere an OFF 'leading' edge that stimulates excitatory subunits and, in turn, the PV-5 cell. The thresholding nonlinearity ensures that the PV-5 cell is activated even in the absence of any dimming—for example, if a compensating, uniform brightening is applied concomitantly to the approach motion (**Fig. 2**). At the expanding edge, excitatory OFF subunits are recruited and respond vigorously to edge motion. By contrast, the slow overall brightening of the receptive field

elicits moderate responses diffusely throughout the ON inhibitory subunits. In a linear system, this global inhibition would cancel out the local excitation. In the nonlinear system, localized but strong inputs have greater impact than weak inputs summed over a wide region.

PV-5 cells make use of rapid inhibition mediated by an electrical synapse. Given the overall slow time courses of retinal responses, it is surprising that inhibition mediated by chemical synapses only is not sufficiently fast to cancel excitation. One explanation for the inhibitory delay may be the rapid inhibition of narrow-field amacrine cells by wide-field amacrine cells. In salamander retina, this has been shown to result in a ~100-ms time difference between excitatory and inhibitory inputs[39]. Indeed, in all inhibitory pathways examined in our work, which use only chemical synapses between bipolar and amacrine cells—namely, the *Cx36*$^{-/-}$ PV-5 cell pathway, the CPP/NBQX-sensitive pathway of the PV-5 cell, and the PV-6 cell pathway—the inhibitory inputs to the ganglion cell were delayed by ~100 ms with respect to the excitatory ones. By contrast, AII amacrine cells do not seem to receive inhibitory inputs from rapid wide-field amacrine cells[40], and, what is more, they receive rapid excitatory inputs through their electrical synapses with bipolar cells. As such, AII amacrine cells combine several properties favorable to their role as part of a spatially narrow, inhibitory pathway used to convey rapid, transient information.

Finally, we suggested the presence of both presynaptic inhibition (acting on OFF bipolar terminals) and postsynaptic inhibition (acting on PV-5 cells) in the PV-5 cell circuit. Postsynaptic inhibition is necessary for approach sensitivity for two reasons: first, because of the considerable scale difference between the size of the subunits—bipolar cells and the AII amacrine cell on the one hand and the PV-5 cell on the other hand—and, second, because of the thresholding that occurs in the bipolar cell–to–ganglion cell information transfer. If inhibition acted only presynaptically, then an inhibitory signal that occurs simultaneously to but in a different location from an excitatory signal would have no effect on the behavior of the PV-5 cell. For example, inhibition caused by the trailing edge of a laterally moving dark object and excitation caused by its leading edge would not couple in the PV-5 ganglion cell. The mechanism of approach sensitivity thus highlights different computational roles for presynaptic inhibition and postsynaptic inhibition.

Multifunctionality in small neural circuits

A key property of the approach-sensitive circuit is the rapid inhibition mediated by the AII amacrine cell: it arrives in time to cancel excitation. In this scenario, the AII amacrine cell fulfills a function very different from the one it is well known for—namely, amplifying rod signals by conveying them to ON and OFF cone pathways[41]. In the present work, we suggest that the AII amacrine cell is also relevant to photopic (daytime) vision, a conclusion that supports recent results in guinea pig[15] and mouse[42].

Our direct demonstration of AII amacrine cell to PV-5 cell connectivity with double-patch experiments and, hence, of the involvement of the AII amacrine cell in the approach-sensitive circuit establishes a functional role of AII amacrine cells in photopic conditions. Notably, neural signals flow along the same circuit module—ON cone bipolar cell through an electrical synapse to AII amacrine cell—under photopic and scotopic conditions, but the direction of the flow is reversed in photopic conditions as compared to scotopic conditions (**Supplementary Fig. 3b**). It thus seems that the nervous system can use the same circuit for entirely different functional purposes under different physiological conditions—an illustration of the efficiency with which biological function can be packed into neural circuits.

METHODS

Methods and any associated references are available in the online version of the paper at http://www.nature.com/natureneuroscience/.

Note: Supplementary information is available on the Nature Neuroscience website.

ACKNOWLEDGMENTS

We are grateful to S. Arber (Friedrich Miescher Institute), D. Paul (Harvard Medical School) and J. Sanes (Harvard University) for providing mouse lines and Robert Margolskee (Mount Sinai School of Medicine) for providing the Gγ13 antibody. We are grateful for the technical assistance of S. Djaffer, B. Gross Scherf and Y. Shimada. We thank members of the Roska lab, P. Lagali, P. Caroni, R. Friedrich and A. Lüthi for comments on the manuscript. The study was supported by Friedrich Miescher Institute funds, a US Office of Naval Research Naval International Cooperative Opportunities in Science and Technology program grant, a Marie Curie Excellence Grant, a Human Frontier Science Program Young Investigator grant, a National Centers of Competence in Research in Genetics grant and a European Union HEALTH-F2-223156 grant to B.R., a Marie Curie Postdoctoral Fellowship to T.A.M., the Centre National de la Recherche Scientifique through the Unité Mixte de Recherche 8550 to R.A.d.S.

AUTHOR CONTRIBUTIONS

T.A.M. performed electrophysiological experiments, designed experiments and model, and wrote manuscript; R.A.S. designed experiments and model and wrote manuscript; S.S. performed immunohistochemistry; T.J.V. performed electrophysiological experiments, G.B.A. performed and designed electrophysiological experiments; and B.R. designed experiments and model and wrote manuscript.

Published online at http://www.nature.com/natureneuroscience/.
Reprints and permissions information is available online at http://npg.nature.com/reprintsandpermissions/.

1. Schiff, W., Caviness, J.A. & Gibson, J.J. Persistent fear responses in rhesus monkeys to the optical stimulus of "looming". *Science* **136**, 982–983 (1962).
2. King, S.M. & Cowey, A. Defensive responses to looming visual stimuli in monkeys with unilateral striate cortex ablation. *Neuropsychologia* **30**, 1017–1024 (1992).
3. Waldeck, R.F. & Gruberg, E.R. Studies on the optic chiasm of the leopard frog. I. Selective loss of visually elicited avoidance behavior after optic chiasm hemisection. *Brain Behav. Evol.* **46**, 84–94 (1995).
4. King, J.G. Jr., Lettvin, J.Y. & Gruberg, E.D. Selective, unilateral, reversible loss of behavioral responses to looming stimuli after injection of tetrodotoxin of cadmium chloride into the frog optic nerve. *Brain Res.* **841**, 20–26 (1999).
5. Ishikane, H., Gangi, M., Honda, S. & Tachibana, M. Synchronized retinal oscillations encode essential information for escape behavior in frogs. *Nat. Neurosci.* **8**, 1087–1095 (2005).
6. Ball, W. & Tronick, E. Infant responses to impending collision: optical and real. *Science* **171**, 818–820 (1971).
7. King, S.M., Dykeman, C., Redgrave, P. & Dean, P. Use of a distracting task to obtain defensive head movements to looming visual stimuli by human adults in a laboratory setting. *Perception* **21**, 245–259 (1992).
8. Hatsopoulos, N., Gabbiani, F. & Laurent, G. Elementary computation of object approach by wide-field visual neuron. *Science* **270**, 1000–1003 (1995).
9. Gabbiani, F., Krapp, H.G. & Laurent, G. Computation of object approach by a wide-field, motion-sensitive neuron. *J. Neurosci.* **19**, 1122–1141 (1999).
10. Gabbiani, F., Cohen, I. & Laurent, G. Time-dependent activation of feed-forward inhibition in a looming-sensitive neuron. *J. Neurophysiol.* **94**, 2150–2161 (2005).
11. Sun, H. & Frost, B.J. Computation of different optical variables of looming objects in pigeon nucleus rotundus neurons. *Nat. Neurosci.* **1**, 296–303 (1998).
12. Huberman, A.D. *et al.* Architecture and activity-mediated refinement of axonal projections from a mosaic of genetically identified retinal ganglion cells. *Neuron* **59**, 425–438 (2008).
13. Kim, I.J., Zhang, Y., Yamagata, M., Meister, M. & Sanes, J.R. Molecular identification of a retinal cell type that responds to upward motion. *Nature* **452**, 478–482 (2008).
14. Haverkamp, S. & Wässle, H. Immunocytochemical analysis of the mouse retina. *J. Comp. Neurol.* **424**, 1–23 (2000).
15. Manookin, M.B., Beaudoin, D.L., Ernst, Z.R., Flagel, L.J. & Demb, J.B. Disinhibition combines with excitation to extend the operating range of the OFF visual pathway in daylight. *J. Neurosci.* **28**, 4136–4150 (2008).
16. Roska, B. & Werblin, F. Vertical interactions across ten parallel, stacked representations in the mammalian retina. *Nature* **410**, 583–587 (2001).
17. Fried, S.I., Münch, T.A. & Werblin, F.S. Mechanisms and circuitry underlying directional selectivity in the retina. *Nature* **420**, 411–414 (2002).
18. Roska, B., Molnar, A. & Werblin, F.S. Parallel processing in retinal ganglion cells: how integration of space-time patterns of excitation and inhibition form the spiking output. *J. Neurophysiol.* **95**, 3810–3822 (2006).

19. Slaughter, M.M. & Miller, R.F. 2-Amino-4-phosphonobutyric acid: a new pharmacological tool for retina research. *Science* **211**, 182–185 (1981).
20. Belgum, J.H., Dvorak, D.R., McReynolds, J.S. & Miyachi, E. Push-pull effect of surround illumination on excitatory and inhibitory inputs to mudpuppy retinal ganglion cells. *J. Physiol. (Lond.)* **388**, 233–243 (1987).
21. McGuire, B.A., Stevens, J.K. & Sterling, P. Microcircuitry of beta ganglion cells in cat retina. *J. Neurosci.* **6**, 907–918 (1986).
22. Mills, S.L., O'Brien, J.J., Li, W., O'Brien, J. & Massey, S.C. Rod pathways in the mammalian retina use connexin 36. *J. Comp. Neurol.* **436**, 336–350 (2001).
23. Feigenspan, A., Teubner, B., Willecke, K. & Weiler, R. Expression of neuronal connexin36 in AII amacrine cells of the mammalian retina. *J. Neurosci.* **21**, 230–239 (2001).
24. Massey, S.C. *et al.* Multiple neuronal connexins in the mammalian retina. *Cell Commun. Adhes.* **10**, 425–430 (2003).
25. Bloomfield, S.A. & Dacheux, R.F. Rod vision: pathways and processing in the mammalian retina. *Prog. Retin. Eye Res.* **20**, 351–384 (2001).
26. Pourcho, R.G. & Goebel, D.J. A combined Golgi and autoradiographic study of (3H)glycine-accumulating amacrine cells in the cat retina. *J. Comp. Neurol.* **233**, 473–480 (1985).
27. Veruki, M.L. & Hartveit, E. Electrical synapses mediate signal transmission in the rod pathway of the mammalian retina. *J. Neurosci.* **22**, 10558–10566 (2002).
28. Geraghty, R.J., Krummenacher, C., Cohen, G.H., Eisenberg, R.J. & Spear, P.G. Entry of alphaherpesviruses mediated by poliovirus receptor-related protein 1 and poliovirus receptor. *Science* **280**, 1618–1620 (1998).
29. Cohen, E.D. & Miller, R.F. The network-selective actions of quinoxalines on the neurocircuitry operations of the rabbit retina. *Brain Res.* **831**, 206–228 (1999).
30. Murphy, G.J. & Rieke, F. Signals and noise in an inhibitory interneuron diverge to control activity in nearby retinal ganglion cells. *Nat. Neurosci.* **11**, 318–326 (2008).
31. Xin, D. & Bloomfield, S.A. Comparison of the responses of AII amacrine cells in the dark- and light-adapted rabbit retina. *Vis. Neurosci.* **16**, 653–665 (1999).
32. Rice, D.S. & Curran, T. Disabled-1 is expressed in type AII amacrine cells in the mouse retina. *J. Comp. Neurol.* **424**, 327–338 (2000).
33. Huang, L. *et al.* G protein subunit G gamma 13 is coexpressed with G alpha o, G beta 3, and G beta 4 in retinal ON bipolar cells. *J. Comp. Neurol.* **455**, 1–10 (2003).
34. Greferath, U., Grunert, U. & Wassle, H. Rod bipolar cells in the mammalian retina show protein kinase C-like immunoreactivity. *J. Comp. Neurol.* **301**, 433–442 (1990).
35. Oyster, C.W. The analysis of image motion by the rabbit retina. *J. Physiol. (Lond.)* **199**, 613–635 (1968).
36. Olveczky, B.P., Baccus, S.A. & Meister, M. Segregation of object and background motion in the retina. *Nature* **423**, 401–408 (2003).
37. Franconeri, S.L. & Simons, D.J. Moving and looming stimuli capture attention. *Percept. Psychophys.* **65**, 999–1010 (2003).
38. Bradley, D.C. & Goyal, M.S. Velocity computation in the primate visual system. *Nat. Rev. Neurosci.* **9**, 686–695 (2008).
39. Roska, B., Nemeth, E. & Werblin, F.S. Response to change is facilitated by a three-neuron disinhibitory pathway in the tiger salamander retina. *J. Neurosci.* **18**, 3451–3459 (1998).
40. Volgyi, B., Xin, D. & Bloomfield, S.A. Feedback inhibition in the inner plexiform layer underlies the surround-mediated responses of AII amacrine cells in the mammalian retina. *J. Physiol. (Lond.)* **539**, 603–614 (2002).
41. Wässle, H. Parallel processing in the mammalian retina. *Nat. Rev. Neurosci.* **5**, 747–757 (2004).
42. Pang, J.J. *et al.* Relative contributions of rod and cone bipolar cell inputs to AII amacrine cell light responses in the mouse retina. *J. Physiol. (Lond.)* **580**, 397–410 (2007).

ONLINE METHODS

Animals. Mice used in our experiments included *Pvalb*^{Cre} × *Thy1*$^{Stp\text{-}EYFP}$, and mice in which the *Cx36*$^{-/-}$ alleles were crossed into the *Pvalb*^{Cre} × *Thy1*$^{Stp\text{-}EYFP}$ background so that PV-5 cells were labeled in a homozygous *Cx36*$^{-/-}$ background. In *Pvalb*^{Cre} mice[43], Cre recombinase is expressed under the control of the parvalbumin locus. In *Thy1*$^{Stp\text{-}EYFP}$ mice[44], EYFP is expressed from a *Thy1* promoter in those cells in which the transcriptional stop sequence has been removed by Cre recombinase[45]. *Cx36*$^{-/-}$ mice[46] are homozygous knockouts for the electrical synapse protein connexin36. All animal procedures were performed in accordance with standard ethical guidelines (European Communities Guidelines on the Care and Use of Laboratory Animals, 86/609/EEC) and were approved by the Veterinary Department of the Canton of Basel-Stadt.

Preparation of retinas. Light-adapted mice were killed by cervical dislocation and decapitation. Eyes were enucleated. The retinas were isolated and the pigment epithelium removed under ambient light in Ringer's medium (in mM: 110 NaCl, 2.5 KCl, 1 $CaCl_2$, 1.6 $MgCl_2$, 10 D-glucose, 22 $NaHCO_3$, bubbled with 5% CO_2/95% O_2, pH 7.4), mounted ganglion cell side up on a filter (MF-membrane, Millipore) that had a 2–3 mm rectangular aperture in the center, and superfused in Ringer's medium at 35–36 °C in the microscope chamber for the duration of the experiment. In this retinal preparation, light responses could be measured for more than 8 h.

Electrophysiology and pharmacology. Spike and current recordings were made with loose cell-attached patch and with whole-cell voltage clamp, respectively, using an Axon Multiclamp 700B amplifier and borosilicate glass electrodes (BF100-50-10, Sutter Instruments) pulled to 7–9 MΩ, and filled with (in mM) 112.5 $CsCH_3SO_3$, 1 $MgSO_4$, 7.8×10^{-3} $CaCl_2$, 0.5 BAPTA, 10 HEPES, 4 ATP-Na_2, 0.5 GTP-Na_3, 5 lidocaine *N*-ethyl bromide (QX314-Br), 7.5 neurobiotin chloride, pH 7.2. In some experiments, either Alexa Fluor 488 (amacrine cell patch) or Lucifer yellow (PV-5 cell patch) was added to the intracellular solution listed above. In the patch electrode for amacrine cells, QX314-Br was substituted by 5 CsCl, and BAPTA by 0.1 EGTA; $CsCH_3SO_3$ was adjusted to 113.7 mM. Excitatory and inhibitory synaptic currents ("excitation" and "inhibition," respectively) were separated by voltage clamping the cell to the equilibrium potential of chloride (−60 mV) and unselective cation channels (0–20 mV), respectively. Data were analyzed offline with Mathematica (Wolfram Research). Spiking rate traces were obtained by convolving spike trains with a gaussian with s.d. σ = 30 ms, except on **Figure 4f**,**g**, where 25-ms flat binning windows were used.

In pharmacological experiments, agents were bath-applied at the following concentrations: 10 μM CPP, 10 μM NBQX, 10 μM or 80 μM APB, 10 μM strychnine, 50 μM curare (tubocurarine chloride), 5 μM SR-95531. All chemicals were obtained from Sigma, with the exception of APB (Calbiochem), ATP (Labforce) and neurobiotin (Vector Laboratories).

Two-photon microscopy. See **Supplementary Figure 6**.

Labeled cells in *Pvalb*^{Cre} × *Thy1*$^{Stp\text{-}EYFP}$ (PV) retinas. Before recording from PV retinas, we obtained an image stack with the two-photon microscope. In the retina, seven ganglion cell types were brightly labeled with EYFP. (Detailed morphological and physiological characterization of all seven classes will be reported elsewhere.) We named these cell classes PV-1 to PV-7, in the order in which their dendritic trees terminate in the IPL, with PV-1 cells arborizing closest to the ganglion cell layer and PV-7 cells closest to the INL. Note that in PV retinas not all members of the seven ganglion cell types are labeled. This is either due to the kinetics of the Cre-*loxP* reaction or due to the mosaic nature of *Thy1* promoter activity.

PV-5 cell targeting. To target PV-5 cells, we first analyzed the two-photon stack. We used two criteria to identify PV-5 cells. The first was cell body size. There were three labeled cell types with large cell bodies (around 20-μm diameter): PV-1, PV-5 and PV-6 cells. To distinguish the three cell types, we followed the course of the dendrites of each of them. We had a marker identifying strata in the IPL because ON-OFF directionally selective cells (PV-2 cells) were also labeled in the PV retina, and these cells arborize in two distinct bands in the IPL. (The same bands were labeled by the ChAT antibodies). These PV-2 bands were bright in the two-photon stacks. The dendrites of one of the cell types with large cell bodies terminated proximally to the proximal PV-2 band. These were the PV-1 cells. The dendrites of the second cell type, PV-6, crossed both PV-2 bands. The dendrites of the third cell type with large cell bodies, the PV-5 cells, terminated between the two PV-2 bands. We filled all recorded cells with neurobiotin and confirmed their size and stratification relative to the ChAT strata (which were the same as the PV-2 strata) *post hoc* (see 'Immunohistochemistry' and 'Confocal analysis'). In every case, the two-photon stratification analysis (relative to the PV-2 strata) was consistent with the confocal *post hoc* stratification analysis. In approximately half the double patch experiments ($n = 16$), we filled the PV-5 cells with Lucifer yellow in addition to neurobiotin. Finally, at the end of every experiment we confirmed the physiological identity of the recorded cell by showing that it received OFF excitation and ON inhibition and that the fast component of the inhibition was not blocked by CPP/NBQX.

AII amacrine cell targeting. We randomly targeted cell bodies in the most proximal row of the INL, where AII amacrine cell bodies are located. On the basis of Dab1 staining (Dab1 is a marker for AII amacrine cells), one-third of all cell bodies in the most proximal row were AII amacrine cells. Therefore, the probability of hitting an AII amacrine cell in this row was 0.33. In the initial recordings, we determined that the cell was an AII amacrine cell only after the retina was fixed, on the basis of Dab1 and streptavidin double staining (neurobiotin was included in the pipette; see below under 'Immunohistochemistry' and 'Confocal analysis') and the characteristic morphology of AII amacrine cells, which includes larger lobules in the OFF strata, smaller terminals in the ON strata and small cell size. In subsequent sets of experiments, we also filled the cells with Alexa Fluor 488, which allowed us to visualize the randomly targeted cells under the two-photon microscope (after recordings).

Statistical analysis. Population data are always reported as mean ± s.e.m. The specific statistical tests used to determine significant differences are reported with the results, and include the *t*-test, the Mann-Whitney rank test and the Kolmogorov-Smirnov test. Significance in all figures is denoted by * for $P < 0.05$, ** for $P < 0.01$, *** for $P < 0.001$ and NS for $P \geq 0.05$.

Light stimulation. See **Supplementary Figure 6**.

Immunohistochemistry. After the experiments, retinas were fixed for 30 min in 4% (wt/vol) paraformaldehyde in PBS (137 mM NaCl, 2.7 mM KCl, 4.3 mM Na_2HPO_4, 1.47 mM KH_2PO_4, pH 7.4) and washed with PBS for at least 1 d at 4 °C. To aid penetration of the antibodies, we froze and thawed the retina three times after cryoprotecting it in 30% (wt/vol) sucrose. All other procedures were carried out at 22–23 °C. After washing the retina in PBS, we blocked it for 1 h in 10% (vol/vol) normal donkey serum (NDS; Chemicon), 1% (wt/vol) bovine serum albumin (BSA), and 0.5% (vol/vol) Triton X-100 in PBS. Primary antibodies were incubated for 7–14 d in 3% (vol/vol) NDS, 1% (wt/vol) BSA, 0.02% (wt/vol) sodium azide and 0.5% (vol/vol) Triton X-100 in PBS. Secondary antibodies incubated for 2 h in 3% (vol/vol) NDS, 1% (wt/vol) BSA, and 0.5% (vol/vol) Triton X-100 in PBS together with streptavidin–Alexa Fluor 555 (Molecular Probes, 1:200) and DAPI (4′,6-diamidine-2-phenylindole dihydrochloride, Roche Diagnostics, 10 μg ml^{-1}). Streptavidin binds to neurobiotin and therefore labels neurobiotin-filled cells. DAPI binds to DNA and therefore labels nuclei. After a final wash in PBS, we embedded the retinas in ProLong Gold antifade (Molecular Probes).

The following set of primary and secondary antibody combinations were used in experiments in which we recorded from only PV ganglion cells: (i) Primary: goat anti–choline acetyltransferase (ChAT, Chemicon, 1:100). Secondary: donkey anti–goat antibodies (immunoglobulin G (IgG) (H+L), Molecular Probes, 1:200, conjugated with Alexa Fluor 633). (ii) Primary: rabbit anti–green fluorescent protein (GFP; Molecular Probes, 1:200). This primary antibody binds not only to GFP but also to EYFP. We used antibody staining for EYFP because fixation decreases EYFP fluorescence. Secondary: donkey anti–rabbit antibodies (Molecular Probes, 1:200, conjugated with Alexa Fluor 488).

The following set of primary and secondary antibody combinations were used to identify amacrine cells as AII amacrine cells (note that neurobiotin was always included in the recording pipettes): (i) Primary: rabbit anti–disabled-1 (Dab1, Chemicon, 1:1,000), a marker for AII amacrine cells. Secondary: donkey anti–rabbit antibodies (IgG (H+L), Jackson, 1:200, conjugated with Cy5). (ii) Primary: sheep anti–GFP (Biogenesis, 1:200). Secondary: donkey anti–sheep antibodies (IgG (H+L), Molecular Probes, 1:200, conjugated with Alexa Fluor 488). This

antibody was used only after paired recordings; it was omitted for retinas in which we had recorded only from amacrine cells.

The following set of primary and secondary antibody combinations were used to identify cells in the distal INL as ON cone bipolar cells after paired recordings from amacrine and PV-5 cells (both neurobiotin filled). (i) Primary: rabbit anti–Gγ13 (R. Margolskee, 1:300). Gγ13 is a marker for ON bipolar cells. Secondary: donkey anti–rabbit antibodies (IgG (H+L), Jackson, 1:200, conjugated with Cy5). (ii) Primary: mouse anti–Protein Kinase C (PKC; BD Bioscience, 1:200). PKC is a marker for rod bipolar cells. Secondary: donkey anti–mouse antibodies (IgG (H+L), Jackson Labs, 1:200, conjugated with DyLight 405). (iii) Primary: sheep anti-GFP (Biogenesis, 1:200). Secondary: donkey anti–sheep (IgG (H+L) Molecular Probes, 1:200, conjugated with Alexa Fluor 488).

Confocal analysis. We analyzed the stained retinas with a Zeiss LSM 510 META confocal microscope. Overall morphologies of the recorded ganglion cells were assessed by using a ×40 oil immersion lens, numerical aperture (NA) 1.3 (**Fig. 1b** bottom panel). The stratification level of neurobiotin-filled ganglion cells (**Fig. 1b** top panel and **Supplementary Fig. 1**) was determined using image stacks acquired with a ×100 oil immersion lens, NA 1.4, at the periphery of the dendritic tree. We plotted first the intensity profiles of the ChAT and neurobiotin staining along the depth of the retina (**Supplementary Fig. 1a**). The depth of the peak of the neurobiotin staining in the IPL relative to the depth of the two IPL peaks of the ChAT staining was used to determine the stratification level of the recorded cell. The depths of the ChAT peaks in the IPL were defined as 0% (proximal ChAT band) and 100% (distal ChAT band). The boundaries of the IPL (relative to the ChAT strata) were defined by determining, first, the peak DAPI fluorescence in the ganglion cell layer and the INL, and, second, the position toward the IPL where the fluorescence intensity of DAPI fell to two-thirds of its peak value. Other confocal stacks were acquired using a ×63 oil immersion lens, NA 1.4 (**Fig. 7g**,**h**,**j–l**), or ×40 oil immersion lens, NA 1.3 (**Fig. 7f**).

Computational model. See **Supplementary Figure 6**.

43. Hippenmeyer, S. *et al*. A developmental switch in the response of DRG neurons to ETS transcription factor signaling. *PLoS Biol.* **3**, e159 (2005).
44. Buffelli, M. *et al*. Genetic evidence that relative synaptic efficacy biases the outcome of synaptic competition. *Nature* **424**, 430–434 (2003).
45. Metzger, D. & Feil, R. Engineering the mouse genome by site-specific recombination. *Curr. Opin. Biotechnol.* **10**, 470–476 (1999).
46. Deans, M.R., Gibson, J.R., Sellitto, C., Connors, B.W. & Paul, D.L. Synchronous activity of inhibitory networks in neocortex requires electrical synapses containing connexin36. *Neuron* **31**, 477–485 (2001).

doi:10.1038/nn.2389